$$d_z = \frac{2\lambda}{NA_{ex}NA_{col}} \quad (42)$$

Since it has been used the signal-idler excitation scheme tuning the excitation wavelengths in order to excite the CARS resonance at around 3047 cm^{-1}, the resulting CARS signal had a wavelength around 715.7 nm, thus substituting to eq. (42) for the two lenses configuration the theoretical axial resolution corresponds to about 22.36 µm for the 10x-4x lenses coupling and to about 11.93 µm for the 20x-4x lenses coupling. The theoretical model thus confirms the elongated shape of the 3D reconstructions of the measured beads.

All the three polystyrene sphere types with nominal diameter of 1 µm, 3 µm and 5 µm have been analysed using the automatic measurement methods adopting a single lenses configuration: the 60x oil immersion objective as focusing lens (UPLSAPO 60XO NA=1.35, Olympus Europe) and a 10x lens (UPLSAPO 10x NA=0.4, Olympus Europe) to collect the forward de-scanned CARS signal. With this lenses configuration the theoretical axial resolution should correspond to about 2.65 µm.

Bandpass filters centred at 716 nm with 43-nm bandwidth (FF01-716/43, Semrock), coupled with shortpass filters with 770nm of cut-off wavelength (FF01-770/SP, Semrock) are used before the detector to further block the residual excitation beams and transmit the CARS signal. The forward de-scanned CARS signal was then focused on a PMT (model R3896, Hamamatsu). In order to prevent sample damages and optimize the output signal the excitation beams were attenuated through a neutral density variable filter wheel (NDC-50C-4M, Thorlabs).

A 3D imaging has been done for all the polystyrene bead types using a Z-step of 0.3 µm for the 3 µm spheres and 0.2 µm for the 1 µm and 5 µm spheres, acquiring image stacks that have been processed using the developed algorithm.

In the table 4.2 and in Fig. 4.14 are shown the results obtained using the developed algorithm (see Appendix - findDiameterAll_.java) related to the largest equivalent diameters measured and the Z-axis diameter computed multiplying the number decreased by one of the images where an object is revealed during the processing of the image stack z-step. The error bars in the plots are related to the standard deviations of the difference between the equivalent diameter and the actual object shape. These errors can represent how the actual shape is close to a real round shape, higher are the errors less rounded is the actual shape.

With this method the measure related to the 3 µm sphere is the closest to the certified value, for the 1 µm sphere the equivalent diameter measured is underestimated while for the 5 µm sphere is slightly overestimated. For such regards the Z-axis diameter, for the 1 µm sphere it has been measured a value lower than theoretical axial resolution, confirming the underestimation of the measure with high probability due to the binary process of images with weak intensity of the CARS signal as the histogram distribution in Fig. 4.9 showed. The Z-axis diameter for the 5 µm sphere is more than three times the reference value.

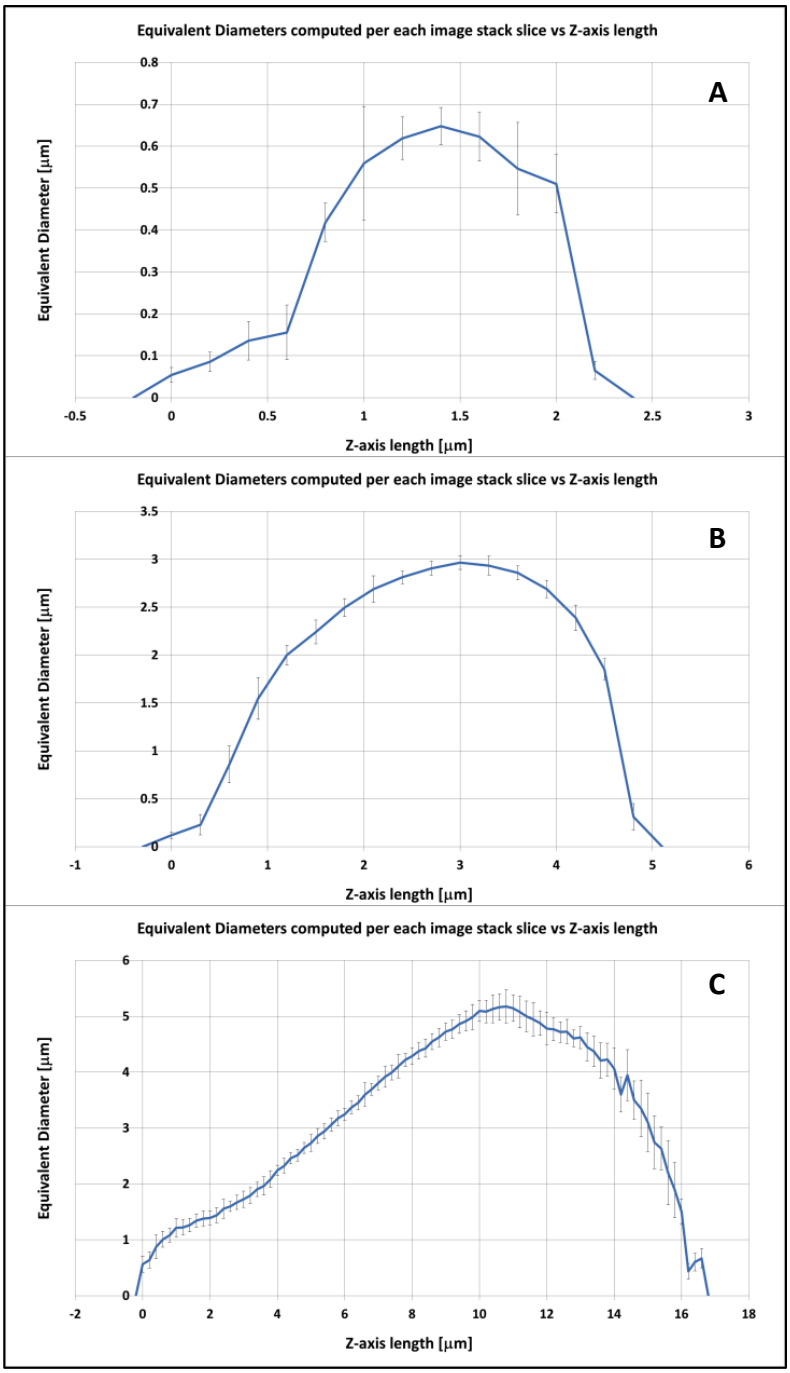

Fig. 4.14 Equivalent diameters computed using the developed algorithm per each image slice along the Z-axis for the 1 µm nominal sphere (A), the 3 µm nominal sphere (B) and the 5 µm nominal sphere.

Bead type	Certified diameter [µm]	Largest computed equivalent diameter [µm]	Error standard deviation [µm]	Z-axis diameter [µm]
1 µm sphere	0.895 ± 0.008	0.65	0.04	2.2
3 µm sphere	2.982 ± 0.016	2.96	0.07	4.8
5 µm sphere	4.983 ± 0.0075	5.17	0.3	16.6

Table 4.2 Equivalent diameters computed using the developed algorithm related to the largest object image slice along the Z-axis for all the analyzed sphere types.

The images related to the measured largest equivalent diameter have been selected together with the XY, ZX, ZY maximum intensity projection images and analysed over a range of threshold values between 5 and 250 and using the autothresholding methods embedded in ImageJ software.

The measures of the object equivalent diameter obtained using the algorithm that I developed on single images have been compared with those obtained using Analyze Particles tool of imageJ, measuring the width and the height of the rectangle that bounds the object in the image, the major and minor axis of the equivalent ellipse that describes at the best the object shape and the Feret's statistical diameter of the object.

The results of these measurements are displayed together with the image that has been processed, the related histogram and the binary images obtained in function of the threshold levels and the employed autothresholding methods. In this way it is possible to clearly see how the image quality and the statistical distribution of the pixels intensities influence dramatically the measurements results, depending by the method used to create binary images and the algorithms utilized to extrapolate the measures.

For such regards the 1 µm nominal sphere in Fig. 4.15, 4.16, 4.17 and 4.18 are displayed the results respectively for the largest object slice in the XY plane and the maximum intensity projections of the XY, ZY, ZX sections.

It is possible to observe that the weakness of the CARS signal of the largest object slice in the XY plane (Fig. 4.15A) is clearly displayed also in its histogram (Fig. 4.15B). This characteristic led to a nearly disappearing of the image with mid-high threshold values (Fig. 4.15C) and all the bead diameter estimators trended towards zero for mid-high threshold values. Only the developed algorithm gave a diameter measure larger than the certified one with low threshold levels (Fig. 4.15D). Feret's diameter and rectangle width and height computed similar results with values higher than those computed with minor and major ellipse axis that showed also similar values. It is possible to observe how the threshold level choice plays a crucial role in the determination of the sphere diameter using binary image processing methods. Autothresholding methods gave heterogeneous results (Fig. 4.15E, 4.15F): Minimum and Shabhag methods led to binary images with no sphere; MinError, Percentile and Triangle methods led to noisy binary images with a strong background signal and a consequent overestimation of the sphere diameter; Default, IsoData, IJ_IsoData, Moments and Otsu methods led to best approximation of the certified sphere diameter using Feret's diameter and the rectangle descriptors; Huang, Li and Mean methods led to best approximation of the certified sphere diameter using the ellipse descriptors; equivalent diameter algorithm gave smaller results than to other estimator results and only the Percentile method led to best approximation of the certified sphere diameter using the developed algorithm.

The maximum intensity projections of the XY, ZY, ZX sections have not a completely dark background due to the noise acquired during the Z-stack measurements, as it is possible to observe watching the related histograms that show no pixels with a zero intensity level (Fig. 4.16B, 4.17B, 4.18B). Moreover histograms show also a little population of pixels with high intensity values, leading to a disappearing of the objects applying mid-high threshold values to create binary images (Fig. 4.16C, 4.17C, 4.18C). With low threshold values instead due to the noisy background level, the binary images are completely black losing all the object shape information, causing a bad functioning of all the sphere diameter estimators.

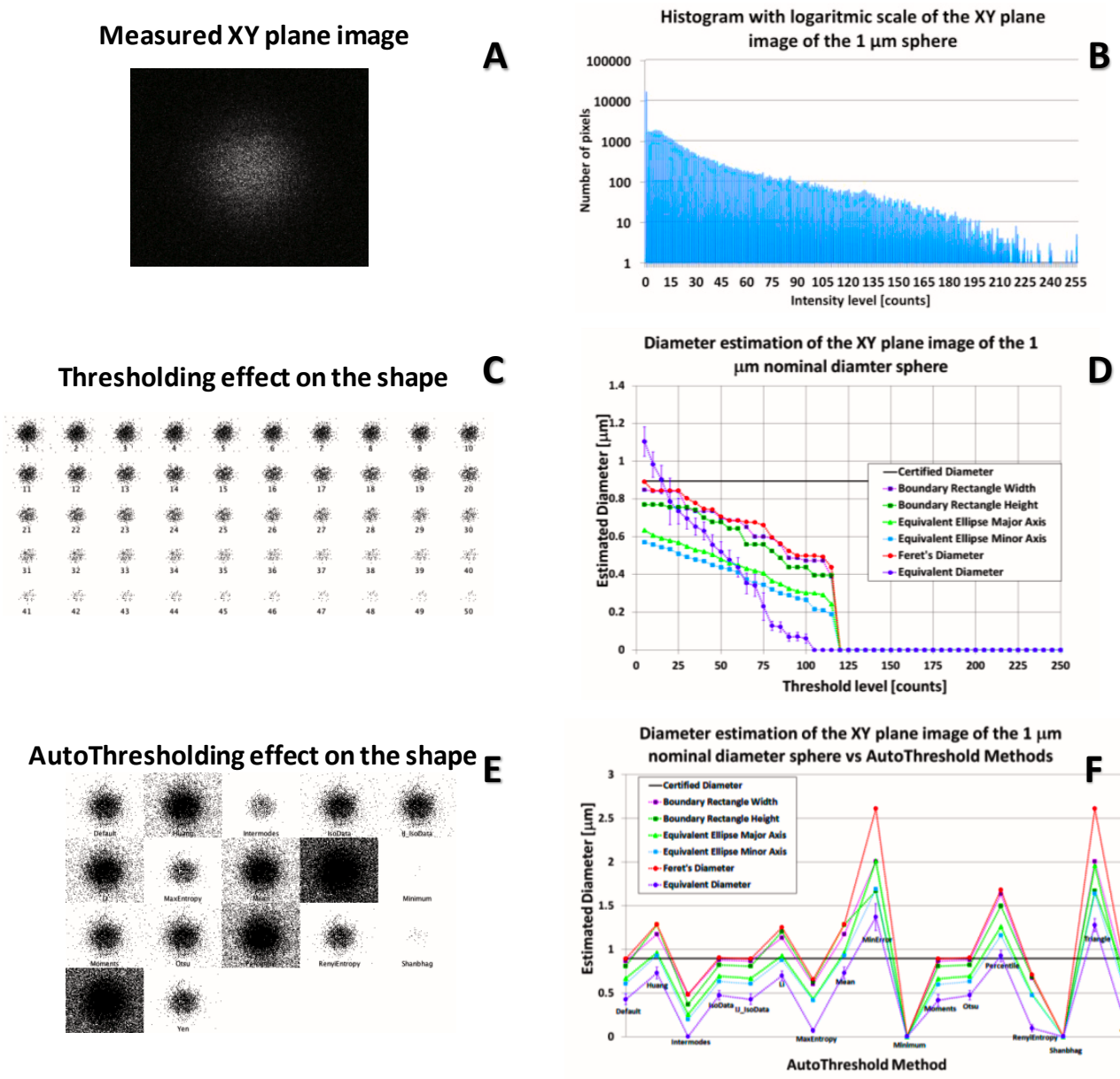

Fig. 4.15 Summary of the results of the image processing of the largest image in the XY plane along the Z-axis for the 1 µm nominal sphere. (A) Processed image. (B) Histogram of the processed image. (C) Thresholding effect on the shape of the object applying increasing thresholding levels. (D) Diameter estimation using the chosen estimator in function of the thresholding level. (E) Binary images created applying all the ImageJ autothresholding methods. (F) Diameter estimation using the chosen estimator in function of the autothresholding methods used.

When the XY section maximum intensity projection has been processed varying the threshold levels and using the autothresholding methods, the developed algorithm gave values lower than those obtained with respectively rectangular descriptors and Feret's diameter and elliptical descriptors. Autothresholding methods gave heterogeneous results (Fig. 4.16E, 4.16F): also in this case Minimum method led to a binary image with no sphere; MinError has not converged creating a black image; Default, IsoData, IJ_IsoData, Moments and Otsu methods led to similar approximations of the certified sphere diameter using all the estimators; MaxEntropy, RenyiEntropy, Shabhag, Triangle and Yen methods led to best approximation of the certified sphere diameter using Feret's diameter and the rectangle descriptors; Li method led to best approximation of the certified sphere diameter using the ellipse descriptors; Huang, Mean and Percentile methods led to best approximation of the certified sphere diameter using the developed algorithm.

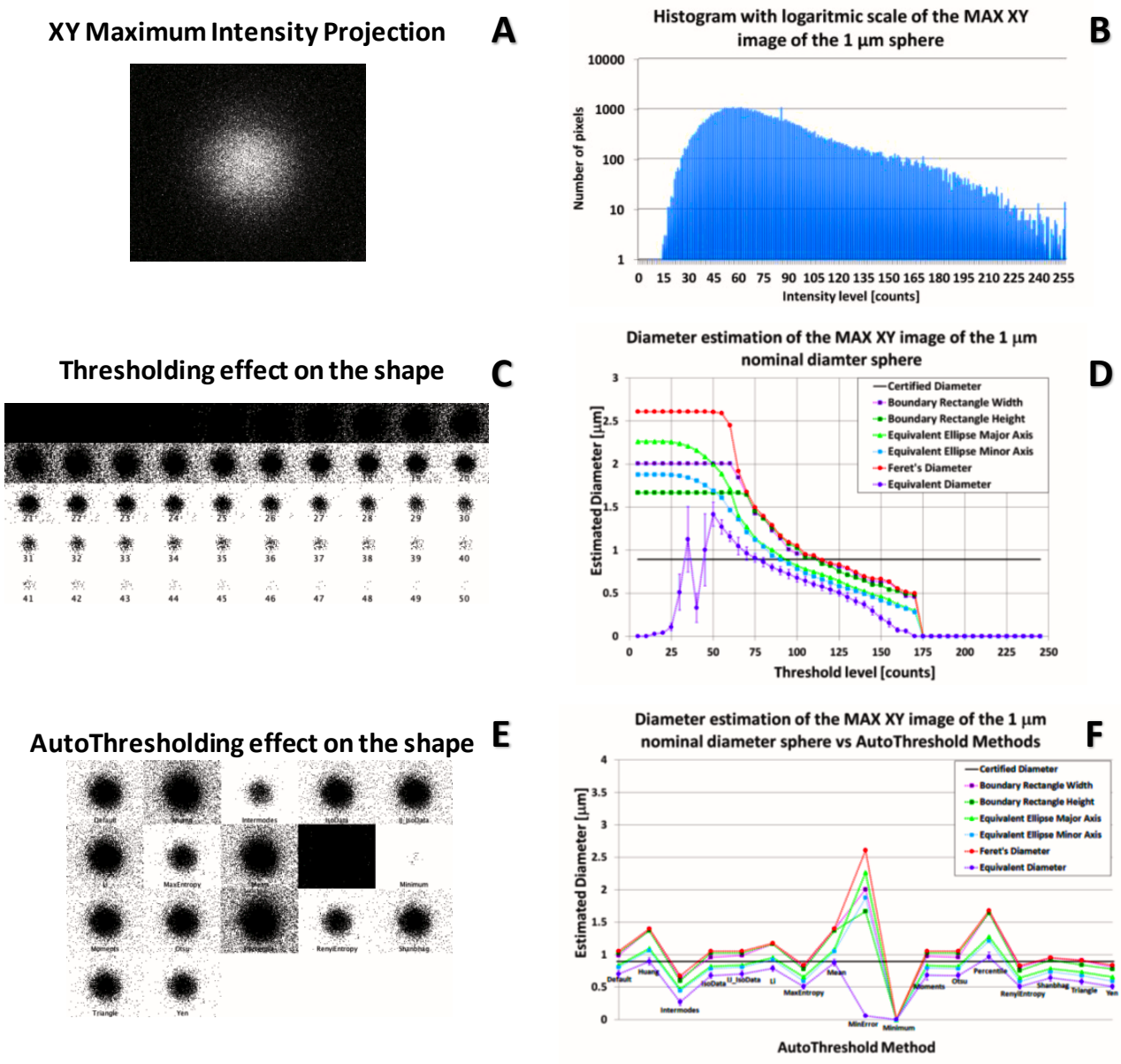

Fig. 4.16 Summary of the results of the image processing of the maximum intensity projection XY section along the Z-axis for the 1 µm nominal sphere. (A) Processed image. (B) Histogram of the processed image. (C) Thresholding effect on the shape of the object applying increasing thresholding levels. (D) Diameter estimation using the chosen estimator in function of the thresholding level. (E) Binary images created applying all the ImageJ autothresholding methods. (F) Diameter estimation using the chosen estimator in function of the autothresholding methods used.

When the ZY and ZX section maximum intensity projections have been processed varying the threshold levels and using the autothresholding methods, the developed algorithm together with the rectangle width and the minor ellipse axis estimators gave values that hardly can evaluate the actual Z-axis measure of the bead. The equivalent diameter algorithm actually estimates an average measure of the XY section diameter and the elongated length, as the high standard deviation computed shows. The rectangle width and the minor ellipse axis estimators gave as a result a measure of the XY section sphere diameter influenced also by the possible tilting of the object along the Z-axis due to lenses misalignments. The actual useful estimators of the length distorted elongated shape that is obtained along the Z-axis when a sphere is imaged are thus the rectangle height, the ellipse major axis and the Feret's diameter. Autothresholding methods gave heterogeneous results (Fig. 4.17E, 4.18E, 4.17F and 4.18F) and observing the obtained binary

images as well as the values of the estimators in function of the threshold levels (Fig. 4.17D and 4.18D), it is reasonable to exclude all the estimated lengths deriving from methods different than MaxEntropy, RenyiEntropy and Yen. The almost constant value of the rectangle height, major ellipse axis and Feret's diameter estimated using all the other autothresholding methods is due in fact to noisy binary images with a strong background signal and a consequent overestimation of the Z-axis length.

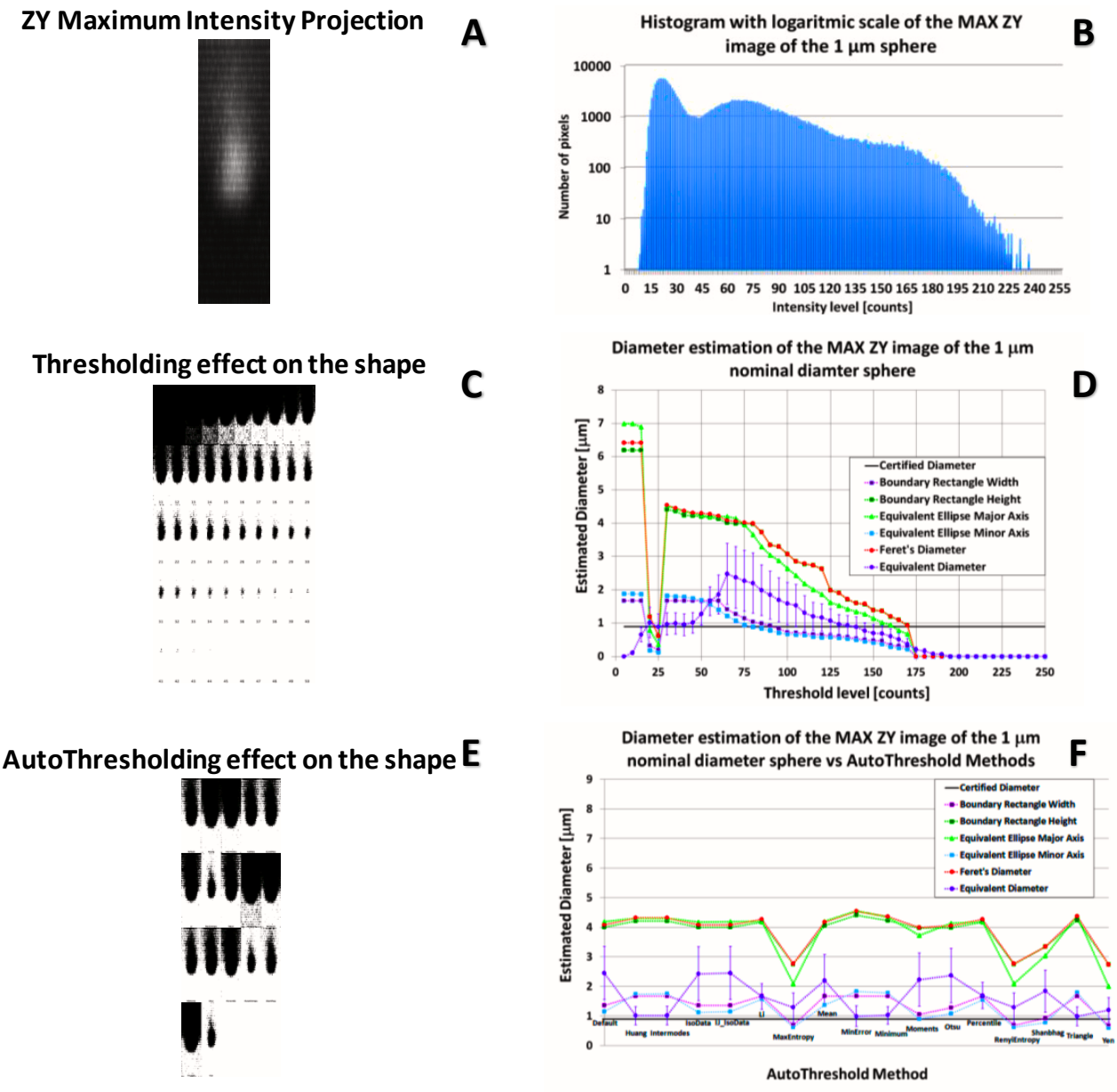

Fig. 4.17 Summary of the results of the image processing of the maximum intensity projection ZY section along the X-axis for the 1 µm nominal sphere. (A) Processed image. (B) Histogram of the processed image. (C) Thresholding effect on the shape of the object applying increasing thresholding levels. (D) Diameter estimation using the chosen estimator in function of the thresholding level. (E) Binary images created applying all the ImageJ autothresholding methods. (F) Diameter estimation using the chosen estimator in function of the autothresholding methods used.

Feret's diameters and the rectangle heights measured through the acceptable methods were about 2.7 µm for both ZX and ZY sections, while major ellipse axis was about 2 µm for ZY section and 2.3 µm for ZX section.

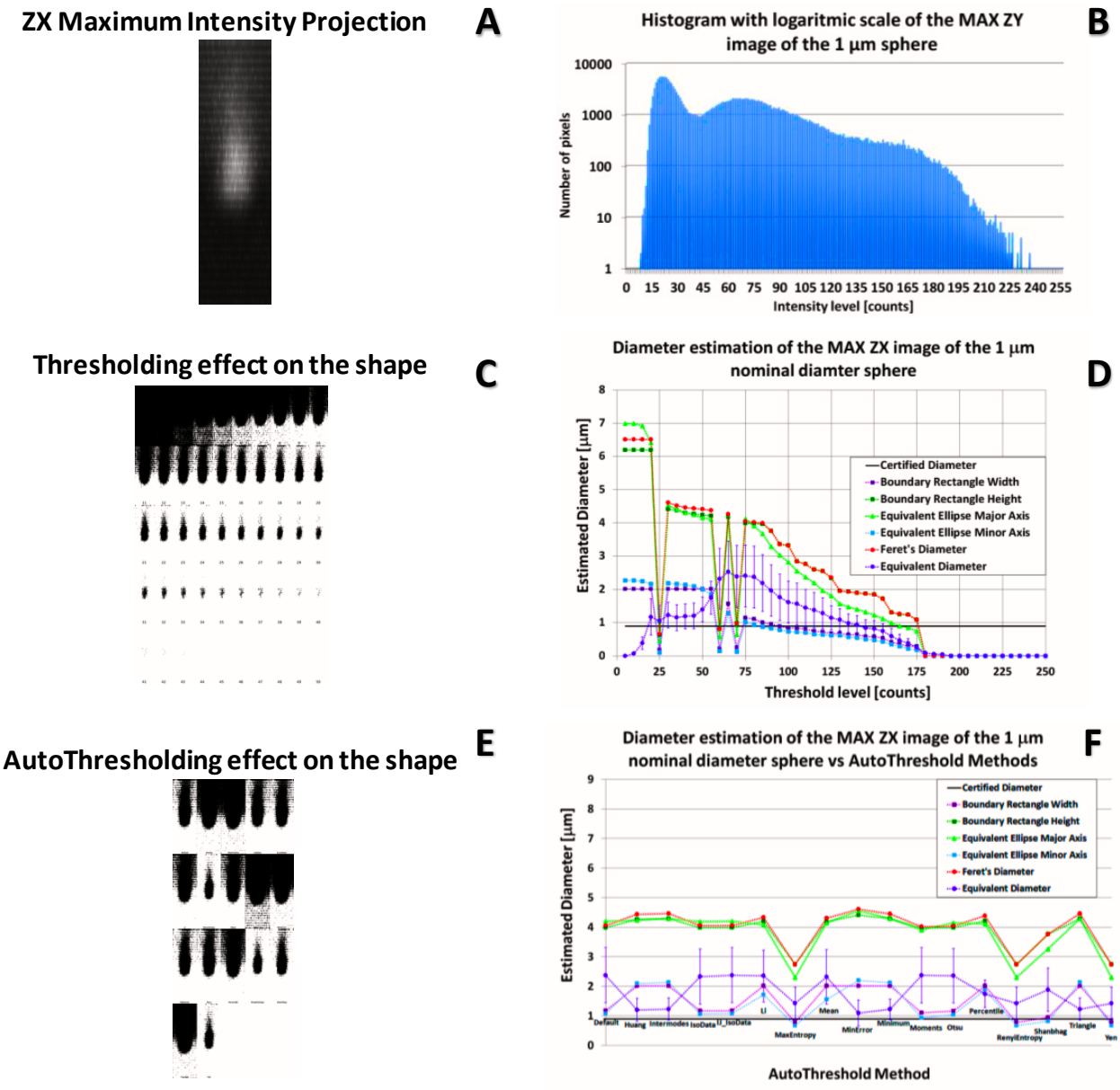

Fig. 4.18 Summary of the results of the image processing of the maximum intensity projection ZX section along the Y-axis for the 1 µm nominal sphere. (A) Processed image. (B) Histogram of the processed image. (C) Thresholding effect on the shape of the object applying increasing thresholding levels. (D) Diameter estimation using the chosen estimator in function of the thresholding level. (E) Binary images created applying all the ImageJ autothresholding methods. (F) Diameter estimation using the chosen estimator in function of the autothresholding methods used.

For such regards the 3 µm nominal sphere in Fig. 4.19, 4.20, 4.21 and 4.22 are displayed the results respectively for the largest object slice in the XY plane and the maximum intensity projections of the XY, ZY, ZX sections.

It is possible to observe from its histogram (Fig. 4.19B) that the CARS signal of the largest object slice in the XY plane (Fig. 4.19A) is stronger than those obtained with the 1 µm nominal sphere. However for high threshold values the object is almost disappeared in the binary image (Fig. 4.19C). Also in this case all the diameter estimators trended towards zero for high threshold values. The developed algorithm gave diameter measures smaller than those expressed by the other estimators (Fig. 4.19D). Feret's diameter and rectangle width and height computed similar results with values higher than those computed with minor

and major ellipse axis that showed also similar values. Autothresholding methods gave heterogeneous results (Fig. 4.19E, 4.19F): Shabhag method led to binary images with an extremely eroded sphere; MinError, Percentile and Triangle methods led to noisy binary images with a strong background signal and a consequent overestimation of the sphere diameter; All the other autothresholding methods led to similar approximations of the certified sphere diameter using all the estimators. Feret's diameter and the rectangle descriptors gave the best approximation of the certified sphere diameter.

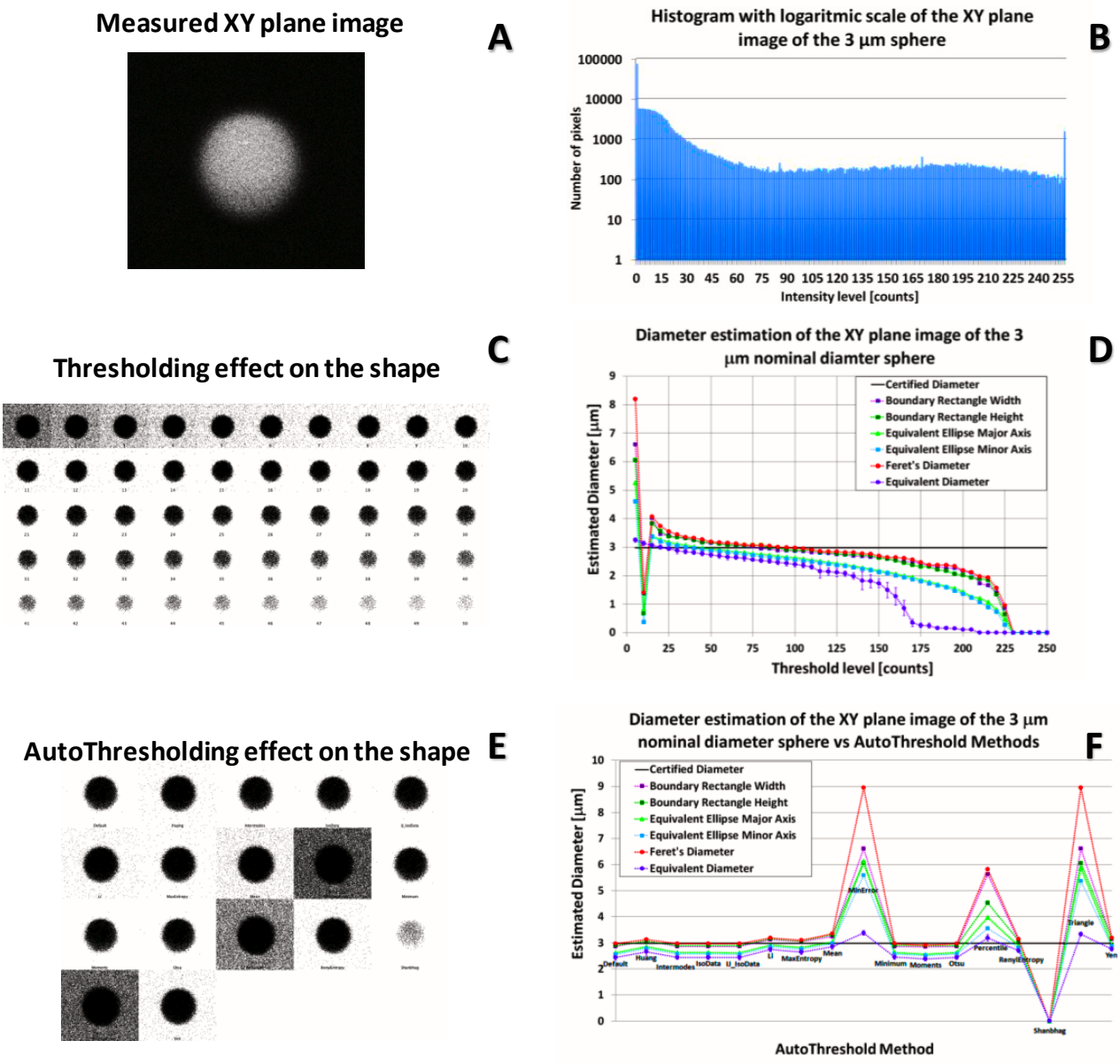

Fig. 4.19 Summary of the results of the image processing of the largest image in the XY plane along the Z-axis for the 3 µm nominal sphere. (A) Processed image. (B) Histogram of the processed image. (C) Thresholding effect on the shape of the object applying increasing thresholding levels. (D) Diameter estimation using the chosen estimator in function of the thresholding level. (E) Binary images created applying all the ImageJ autothresholding methods. (F) Diameter estimation using the chosen estimator in function of the autothresholding methods used.

Also in this case the maximum intensity projections of the XY, ZY, ZX sections have not a completely dark background due to the noise acquired during the Z-stack measurements, as it is possible to observe watching the related histograms that show no pixel with low intensity levels (Fig. 4.20B, 4.21B, 4.22B). Moreover histograms of ZY and ZX section show also a little population of pixels with high intensity values,

leading to a disappearing of the objects applying high threshold values to create binary images (Fig. 4.20C, 4.21C, 4.22C). With low threshold values instead due to the noisy background level, the binary images are completely black losing all the object shape information, causing a bad functioning of all the sphere diameter estimators.

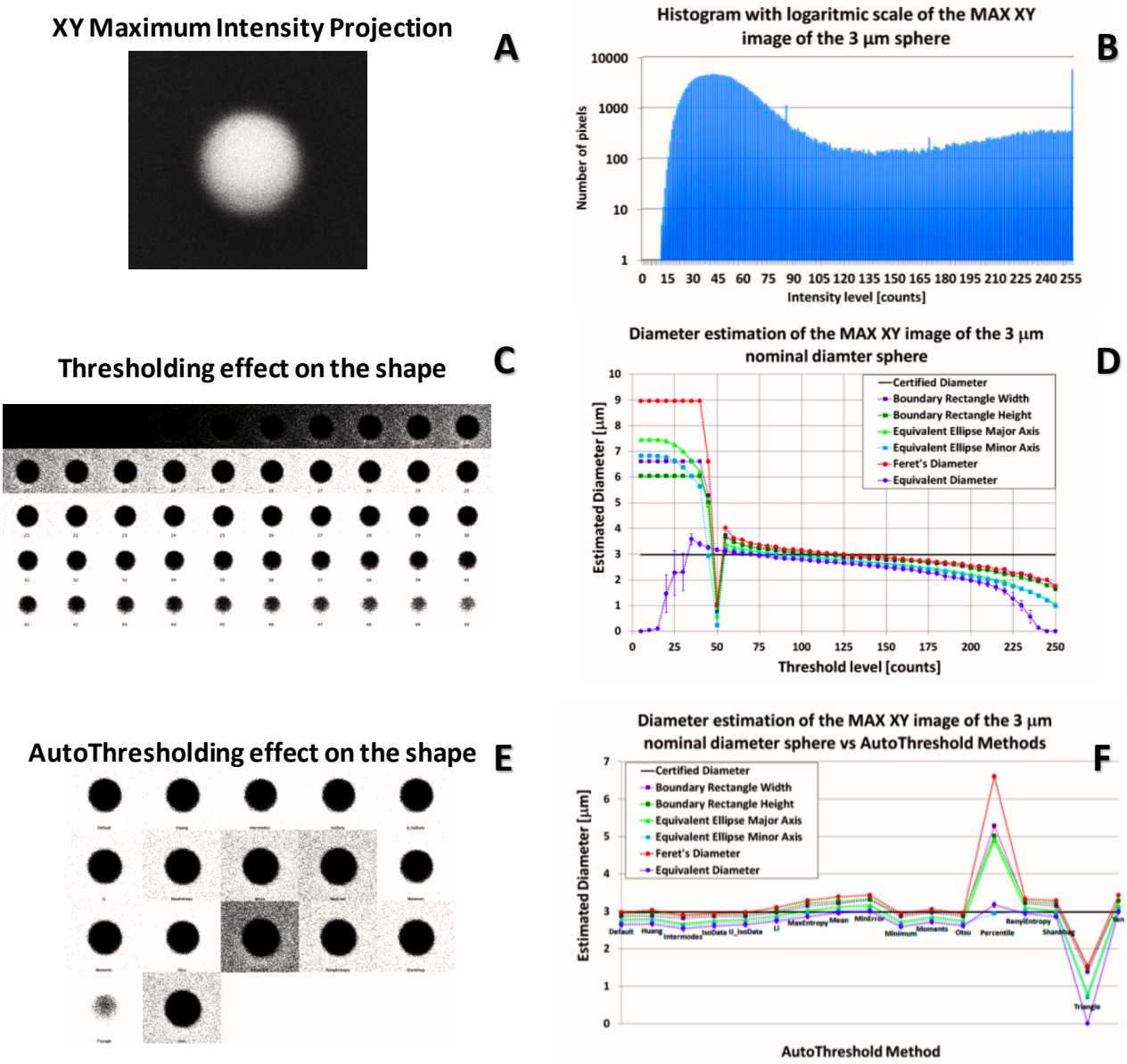

Fig. 4.20 Summary of the results of the image processing of the maximum intensity projection XY section along the Z-axis for the 3 µm nominal sphere. (A) Processed image. (B) Histogram of the processed image. (C) Thresholding effect on the shape of the object applying increasing thresholding levels. (D) Diameter estimation using the chosen estimator in function of the thresholding level. (E) Binary images created applying all the ImageJ autothresholding methods. (F) Diameter estimation using the chosen estimator in function of the autothresholding methods used.

When the XY section maximum intensity projection has been processed varying the threshold levels and using the autothresholding methods, the developed algorithm gave values lower than those obtained with respectively rectangular descriptors and Feret's diameter and elliptical descriptors.

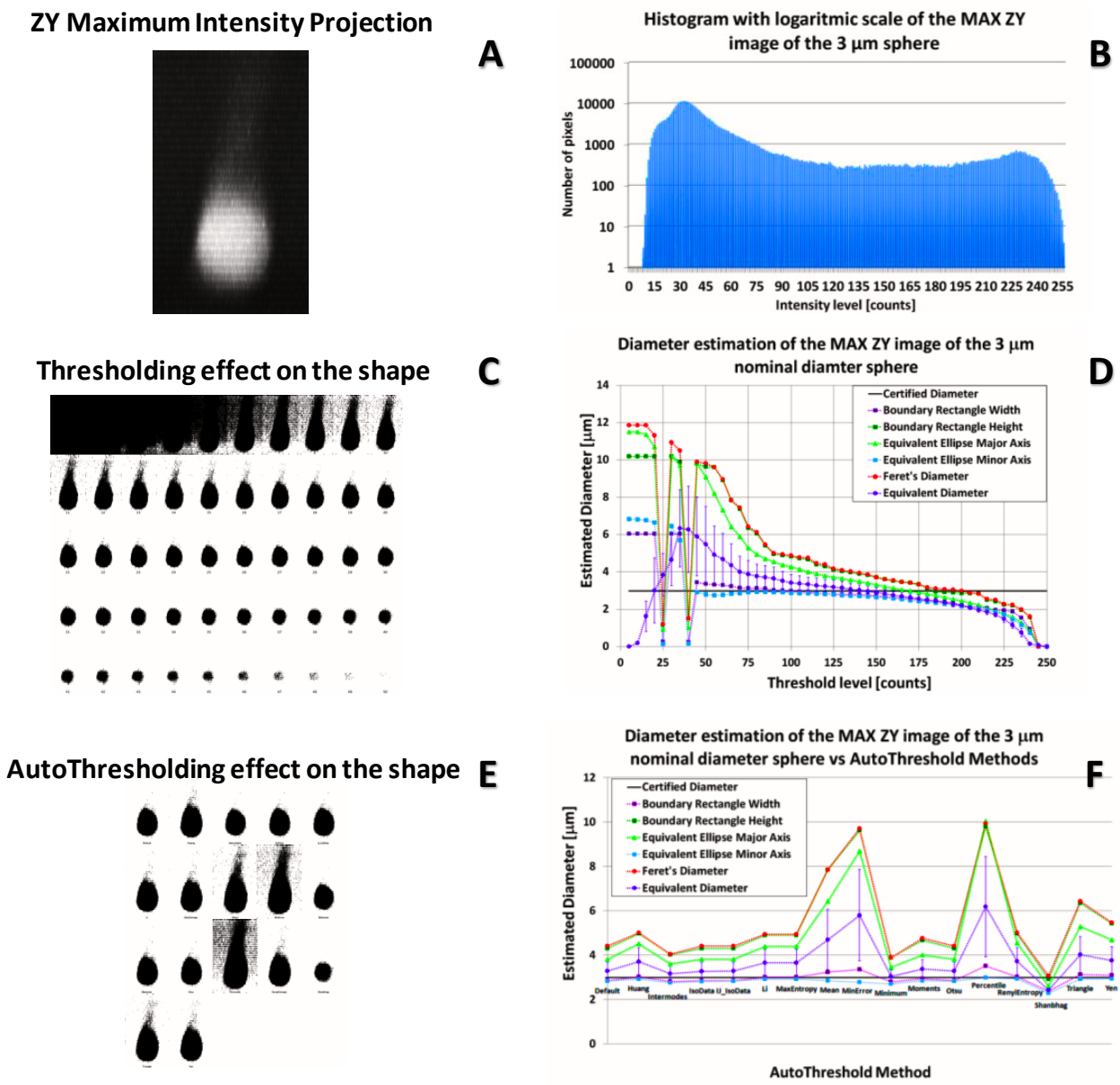

Fig. 4.21 Summary of the results of the image processing of the maximum intensity projection ZY section along the X-axis for the 3 µm nominal sphere. (A) Processed image. (B) Histogram of the processed image. (C) Thresholding effect on the shape of the object applying increasing thresholding levels. (D) Diameter estimation using the chosen estimator in function of the thresholding level. (E) Binary images created applying all the ImageJ autothresholding methods. (F) Diameter estimation using the chosen estimator in function of the autothresholding methods used.

Excluding Triangle and Percentile methods, autothresholding methods gave quite homogeneous results (Fig. 4.20E, 4.20F): Triangle method led to a binary image with a strongly eroded sphere; Percentile method create a binary image with a strong background contribution; Default, Huang, Intermode, IsoData, IJ_IsoData, Minimum, Moments and Otsu methods led to best approximation of the certified sphere diameter using Feret's diameter and the rectangle descriptors; MaxEntropy, Mean, MinError, RenyiEntropy, Shanbhag and Yen methods led to best approximation of the certified sphere diameter using the developed algorithm and the ellipse descriptors.

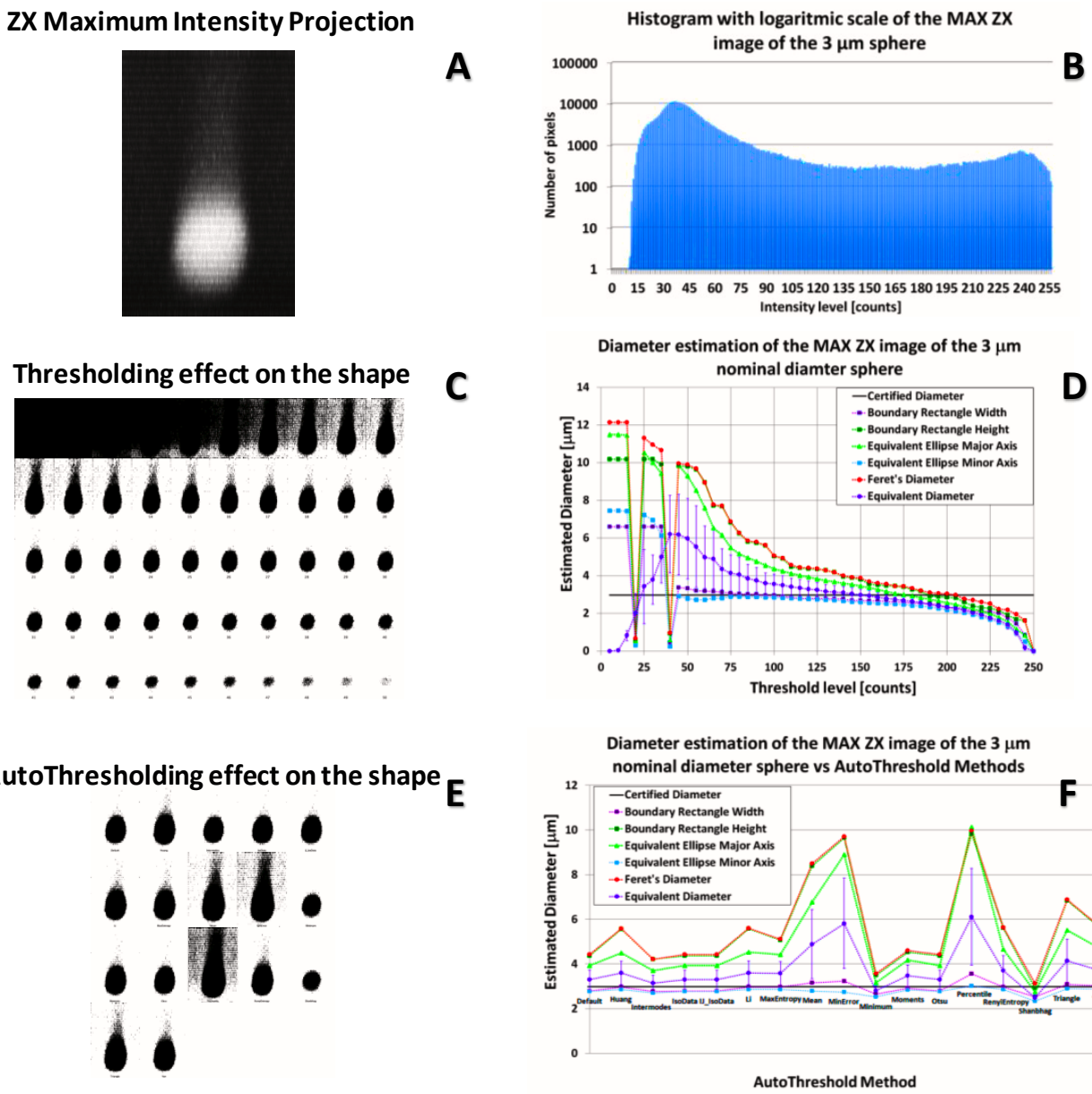

Fig. 4.22 Summary of the results of the image processing of the maximum intensity projection ZX section along the Y-axis for the 3 µm nominal sphere. (A) Processed image. (B) Histogram of the processed image. (C) Thresholding effect on the shape of the object applying increasing thresholding levels. (D) Diameter estimation using the chosen estimator in function of the thresholding level. (E) Binary images created applying all the ImageJ autothresholding methods. (F) Diameter estimation using the chosen estimator in function of the autothresholding methods used.

As for the case of 1 µm nominal sphere, when the ZY and ZX section maximum intensity projections have been processed varying the threshold levels and using the autothresholding methods, the developed algorithm together with the rectangle width and the minor ellipse axis estimators gave values that cannot evaluate the actual Z-axis elongation length of the bead seen that rectangle width and the minor ellipse axis estimators are strongly referred to XY plane. The actual useful estimators of the Z-axis elongation length are thus the rectangle height, the ellipse major axis and the Feret's diameter.

However in this case using the rectangle width and the minor ellipse axis estimators to measure the XY plane diameter from the ZX and ZY sections gave the results less influenced by the threshold level for a larger range (from about 70 counts to 140 counts) than when the XY sections were analysed.

Rectangle height and Feret's diameter were highly correlated with similar values using all autothresholding methods that gave in general quite heterogeneous results (Fig. 4.21E, 4.22E, 4.21F and 4.22F). Observing the values of the estimators in function of the threshold levels (Fig. 4.21D, 4.22D) and the obtained binary images (Fig. 4.21C, 4.22C, 4.21E and 4.22E) it is reasonable to exclude all the estimated lengths deriving from Mean, MinError and Percentile methods. Triangle method gave the highest estimations in both ZY and ZX sections of the Z-axis length elongation, while Shanbhag method gave the lowest.

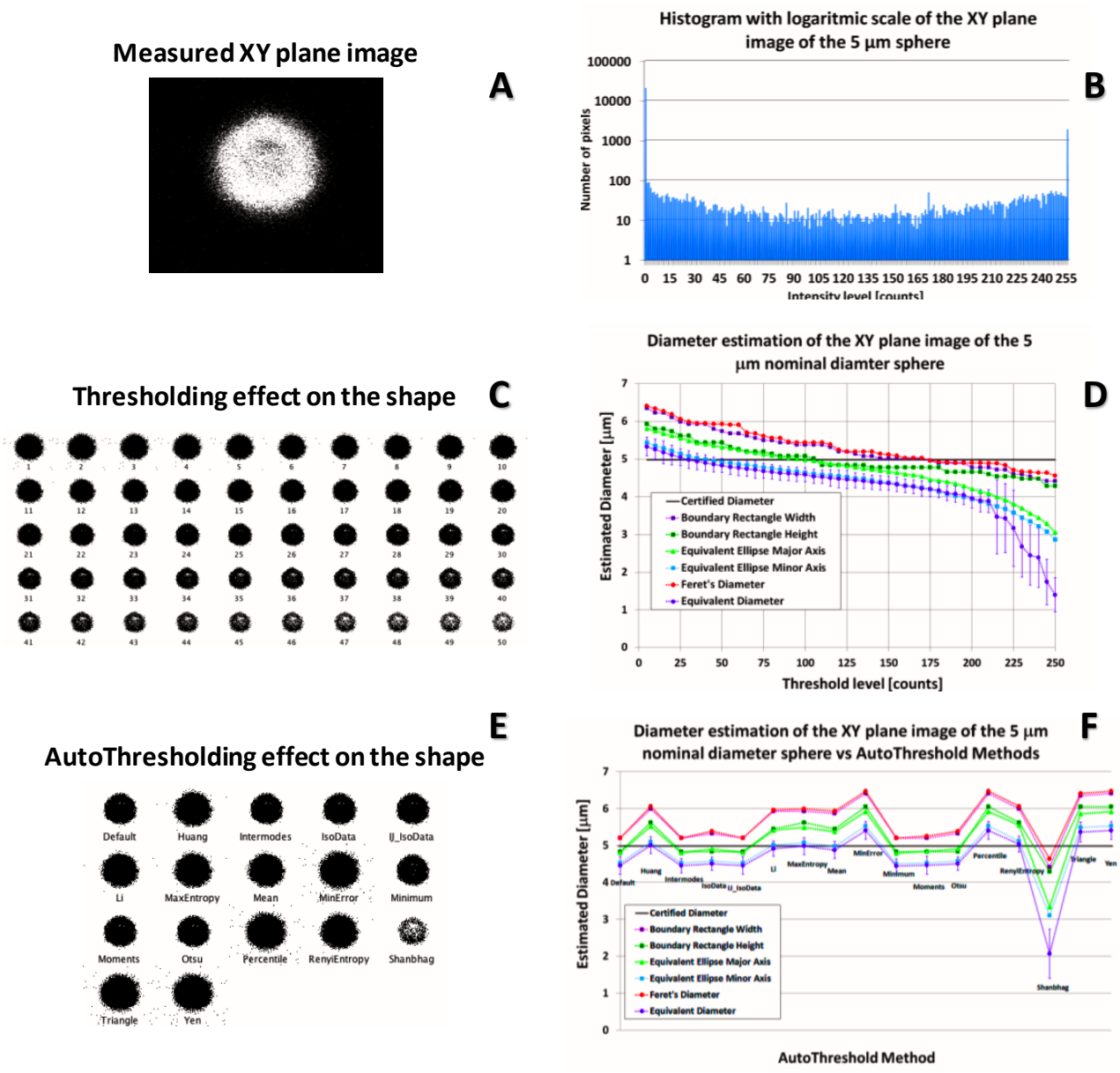

Fig. 4.23 Summary of the results of the image processing of the largest image in the XY plane along the Z-axis for the 5 µm nominal sphere. (A) Processed image. (B) Histogram of the processed image. (C) Thresholding effect on the shape of the object applying increasing thresholding levels. (D) Diameter estimation using the chosen estimator in function of the thresholding level. (E) Binary images created applying all the ImageJ autothresholding methods. (F) Diameter estimation using the chosen estimator in function of the autothresholding methods used.

Huang, Li, MaxEntropy, Moments, RenyiEntropy and Yen methods led to an estimation of the rectangle height (and the Feret's diameter) for both ZY and ZX sections of about 5 µm and 5.5 µm respectively and a major ellipse axis for both ZY and ZX sections of about 4.5 µm. Default, Intermodes, isoData, IJ_IsoData, Moments and Otsu methods led to an estimation of the rectangle height (and the Feret's diameter) for

both ZY and ZX sections of about 4.5 µm and a major ellipse axis for both ZY and ZX sections of about 3.7 µm and 4 µm respectively. Minimum and Shabhag methods led to the best approximation of the certified diameter.

Excluding Shabhag method all the autothresholding methods led to a good approximation of the certified diameter using the minor ellipse axis estimator.

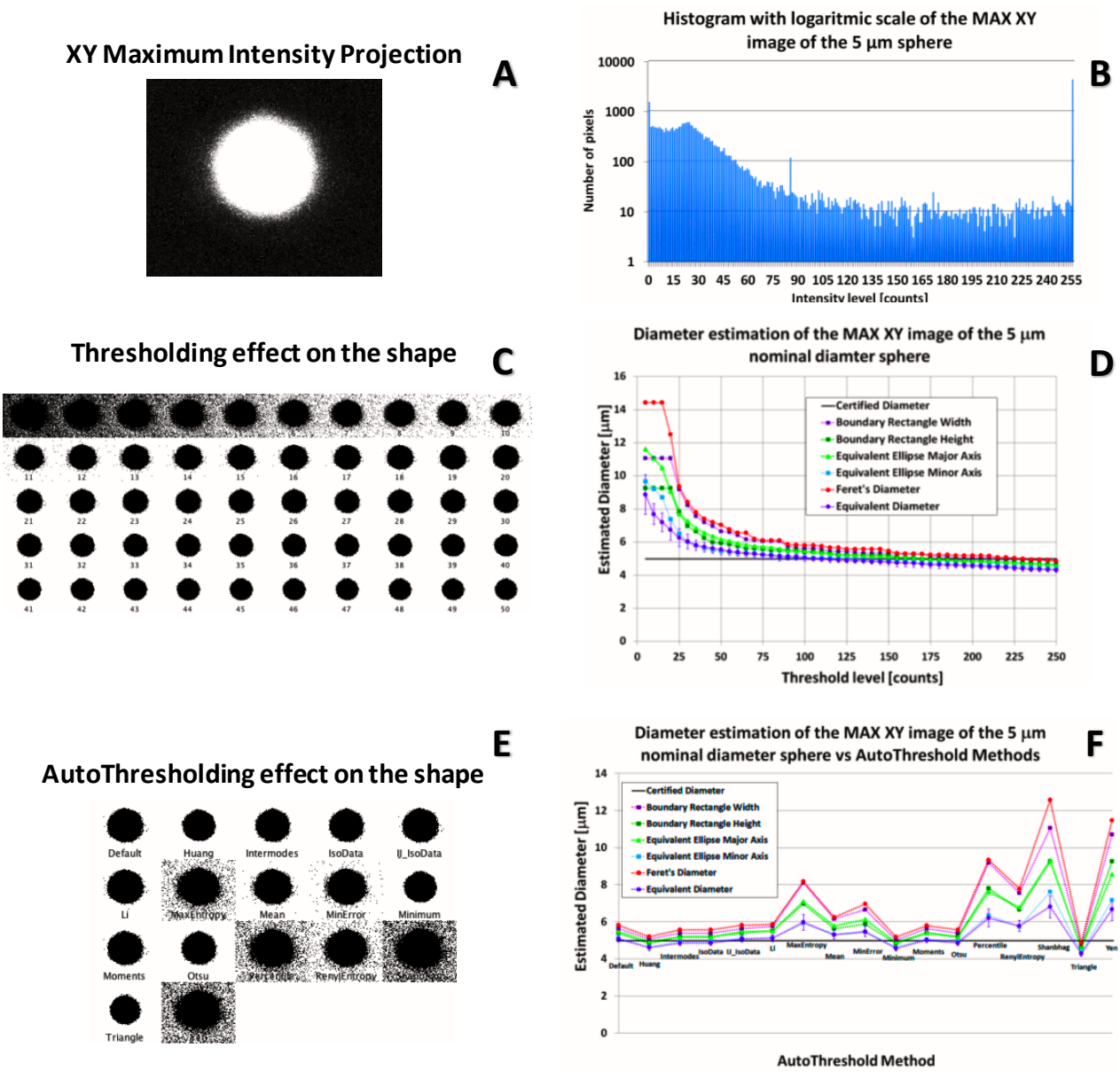

Fig. 4.24 Summary of the results of the image processing of the maximum intensity projection XY section along the Z-axis for the 5 µm nominal sphere. (A) Processed image. (B) Histogram of the processed image. (C) Thresholding effect on the shape of the object applying increasing thresholding levels. (D) Diameter estimation using the chosen estimator in function of the thresholding level. (E) Binary images created applying all the ImageJ autothresholding methods. (F) Diameter estimation using the chosen estimator in function of the autothresholding methods used.

For such regards the 5 µm nominal sphere in Fig. 4.23, 4.24, 4.25 and 4.26 are displayed the results respectively for the largest object slice in the XY plane and the maximum intensity projections of the XY, ZY, ZX sections.

It is possible to observe from its histogram (Fig. 4.23B) that the CARS signal of the largest object slice in the XY plane (Fig. 4.23A) is quite uniform and bimodal distribution is slightly appreciable. The presence of a large number of saturated pixels in the image made the object still visible in the binary image for high threshold values, even if the centre slightly disappeared (Fig. 4.23C). In this case all the diameter estimators trended downward for high threshold values but without reaching a zero value. The developed algorithm gave a diameter measure generally smaller than those expressed by the other estimators (Fig. 4.23D). For threshold level lower than 150 counts Feret's diameter and rectangle width extrapolated similar results. In the same range also major ellipse axis and rectangle height gave similar results. Instead, for threshold levels lower than 210 counts equivalent diameter results were similar to those of minor ellipse axis.

Autothresholding methods gave heterogeneous results (Fig. 4.23E, 4.23F): Shabhag method led to binary images with the most eroded sphere; MinError, Percentile, Triangle and Yen methods led to binary images with larger size objects with consequent overestimation of the sphere diameter; Huang, Li, MaxEntropy, Mean and RenyiEntropy methods led to best approximations of the certified sphere diameter using the developed algorithm and the minor ellipse axis estimators.

Default, Intermodes, IsoData, IJ_IsoData, Minimum, Moments, Otsu methods led to best approximations of the certified sphere diameter using the major ellipse axis and rectangle height estimators. Feret's diameter and rectangle width estimators showed overestimation of the measure with respect to the certified measure using all the autothresholding methods.

When the XY section maximum intensity projection has been processed varying the threshold levels and using the autothresholding methods, the developed algorithm gave lower values than those obtained with all the other size descriptors used. With respect to the other polystyrene spheres measured, the trend of variation in function of the threshold value has a lower slope, except for lower threshold values due to the noisy background that disturbs the diameter extrapolations with all the estimators. Also in this case the estimators gave results that were similar for Feret's diameter and the rectangle width, for rectangle height and ellipse major axis and for equivalent diameter and minor ellipse axis.

Autothresholding methods gave quite heterogeneous results (Fig. 4.24E, 4.24F): MaxEntropy, Percentile, RenyiEntropy, Shabhag and Yen methods led to binary images with larger size objects with consequent overestimation of the sphere diameter; Default, Intermodes, IsoData, IJ_IsoData, Li, Moments and Otsu methods led to best approximations of the certified sphere diameter using the developed algorithm and the minor ellipse axis estimators. Huang and Minimum methods led to best approximations of the certified sphere diameter using the major ellipse axis and rectangle height estimators. Huang, Minimum and Triangle methods led to best approximations of the certified sphere diameter using Feret's diameter and rectangle width estimators.

As it was previously said, when the ZY and ZX section maximum intensity projections have been processed varying the threshold levels and using the autothresholding methods, the developed algorithm together with the rectangle width and the minor ellipse axis estimators gave values that cannot evaluate the actual Z-axis elongation length of the bead seen that rectangle width and the minor ellipse axis estimators are referred strongly to XY plane. The actual useful estimators of the Z-axis elongation length are thus the rectangle height, the ellipse major axis and the Feret's diameter.

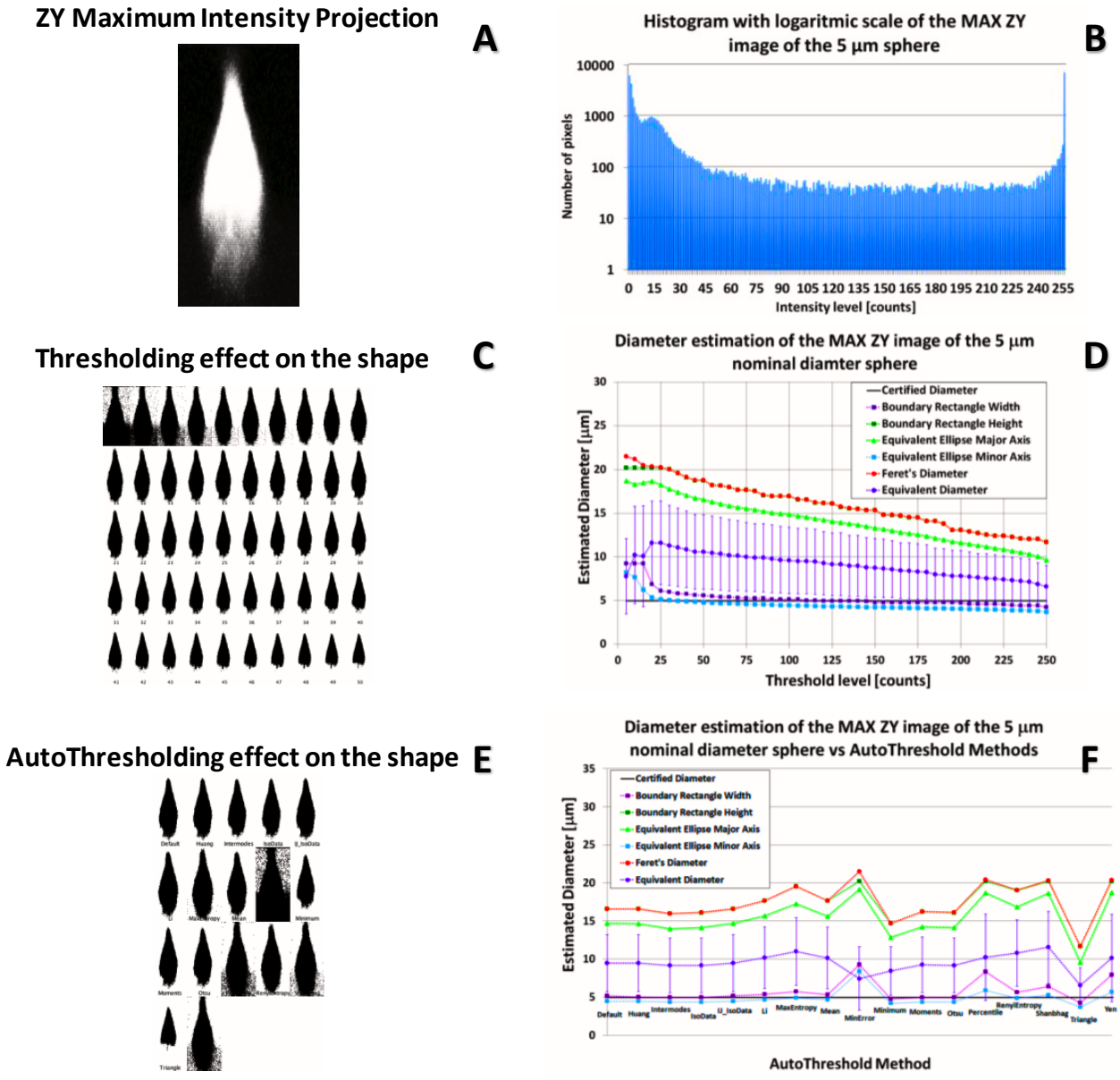

Fig. 4.25 Summary of the results of the image processing of the maximum intensity projection ZY section along the X-axis for the 5 µm nominal sphere. (A) Processed image. (B) Histogram of the processed image. (C) Thresholding effect on the shape of the object applying increasing thresholding levels. (D) Diameter estimation using the chosen estimator in function of the thresholding level. (E) Binary images created applying all the ImageJ autothresholding methods. (F) Diameter estimation using the chosen estimator in function of the autothresholding methods used.

However also in this case using the rectangle width and the minor ellipse axis estimators to measure the XY plane diameter from the ZX and ZY sections gave results less influenced by the threshold level due to a lower slope in the variation of the estimation in function of the threshold levels.

Rectangle height and Feret's diameter were highly correlated with similar values using all autothresholding methods that gave in general quite heterogeneous results (Fig. 4.25E, 4.26E, 4.25F and 4.26F). Observing the values of the estimators in function of the threshold levels (Fig. 4.25D, 4.26D) and the obtained binary images (Fig. 4.25C, 4.26C, 4.25E and 4.26E) it is reasonable to exclude all the estimated lengths deriving from MaxEntropy, MinError, Percentile, RenyiEntropy, Shanbhag, Triangle and Yen methods. Li and Mean methods gave the highest estimations of the rectangle height (and the Feret's diameter) for both ZY and ZX